

Surface electronic structure of the strongly correlated compound CeCo_2P_2

Shuai-Kang Zhang¹, Zhao-Yi Zeng^{2,*}, Yuan-Ji Xu^{3,†}, Xiang-Rong Chen^{1,‡} and Guang-Fu Ji⁴

¹College of Physics, Sichuan University, Chengdu 610064, China

²College of Physics and Electronic Engineering, Chongqing Normal University, Chongqing 400047, China

³Institute for Applied Physics, University of Science and Technology Beijing, Beijing 100083, China

⁴National Key Laboratory for Shock Wave and Detonation Physics Research, Institute of Fluid Physics, China Academy of Engineering Physics (CAEP), Mianyang 621900, China



(Received 14 November 2022; revised 2 April 2023; accepted 16 May 2023; published 30 May 2023)

The f electrons near the surface of strongly correlated materials show unique properties due to the different environments from those in bulk. Here, we used the density functional theory (DFT) and DFT+dynamical mean field theory method to study the surface electronic structures of the P- and Ce-terminated layer structure of CeCo_2P_2 . First, we find that the surface states of the paramagnetic P-terminated slab exhibit heavy-fermion behavior. Second, the flat bands of surface Ce- $4f_{5/2}$ in the P-terminated slab was closer to the Fermi level (E_F) than that of Ce- $4f_{5/2}$ in bulk and hybridized with Co- $3d$ conductive bands at low temperature. However, the surface Ce of the Ce-terminated slab was closer to the atomic state because it is in contact with the vacuum, and its strength of hybridization is lower than that of the P-terminated slab, leading to a weaker Kondo resonance peak near E_F . Third, the relaxation of the surface adjusts the dispersion of the bands and enhances the Kondo resonance for the P-terminated slab. Finally, after considering the antiferromagnetic order of Co, we found that the band structure was closer to the experiment results. These results show that CeCo_2P_2 is an ideal material for studying interlayer coupling between the two-dimensional Kondo lattice and magnetic layers.

DOI: [10.1103/PhysRevB.107.195440](https://doi.org/10.1103/PhysRevB.107.195440)

I. INTRODUCTION

Many strange phenomena in strongly correlated systems, such as Kondo effect and superconductivity, are surface sensitive due to their low energy scale [1–9]. Thus, a lot of attention has been paid to the surface states of strongly correlated systems [10–17]. In recent years, due to the development of surface-sensitive experimental techniques, especially angle-resolved photoemission spectroscopy (ARPES), some high-quality experimental results of surfaces electronic states of strong correlated materials, such as CeRh_2Si_2 , SmB_6 , and CeIrIn_5 , were reported [18–23]. Furthermore, many studies have shown that the behaviors of the f electrons near the surface are different from those of the bulk, due to the change of electronic environment, the relaxation and reconstruction, the destruction of inversion symmetry, the change of crystal field, and so on [19,20,24–29]. Therefore, some strongly correlated layered materials have become excellent candidates for studying the surface effect on the f -electron properties.

As shown in Fig. 1(a), a CeCo_2P_2 crystal has a body-centered tetragonal ThCr_2Si_2 layered structure with the space group $I4/mmm$ (No. 139) [23,30], where Co ions bond with P ions and form a Co-P layer. Each Co-P layer is alternately arranged with the Ce-ion layer along the c axis. Co ions are completely ferromagnetic arranged on the a - b plane and

antiferromagnetic (AFM) order along the c axis with a higher Néel temperature $T_N = 440$ K. However, the heat capacity measurements showed that the Sommerfeld coefficients in CeCo_2P_2 ($\gamma = 4.8 \pm 0.1$ mJ/mol K²) are even smaller than those in LaCo_2P_2 ($\gamma = 18.0 \pm 0.2$ mJ/mol K²) [23,31], and there is no strong Kondo interaction in the bulk of CeCo_2P_2 . In addition, Xu *et al.* [32] studied the topological surface states of CeCo_2P_2 based on first-principles calculations, and their results show that CeCo_2P_2 is a magnetic topological material. Recently, Poelchen *et al.* [23] studied the surface electronic state of CeCo_2P_2 through an ARPES experiment and density functional theory (DFT) calculations. The band structure observed via ARPES at low temperature showed that there were flat bands near E_F , and a sharp peak of $4f_{5/2}$ near E_F was also observed in the photoemission spectrum integrated over the ARPES data. However, the flat bands and the smaller Sommerfeld coefficient γ of CeCo_2P_2 are incompatible. These ARPES results indicate that the surface state Ce- $4f$ has a heavy-fermion behavior that the bulk Ce- $4f$ does not have. However, these DFT results do not describe the heavy-fermion characteristics of the surface Ce- $4f$ well because the DFT method cannot describe the Kondo effect well. In addition, the influence of the AFM order of Co ions on the heavy-fermion behavior of the surface state also needs further studies.

In this paper, we build P- and Ce-terminated slabs and investigate their electronic structures by DFT and DFT+dynamical mean field theory (DMFT) methods. First, for the Ce-terminated slab, the energy level of surface Ce- $4f_{5/2}$ is much higher than that of the bulk because surface Ce ions are

*zhaoyizeng@cqu.edu.cn

†yuanjixu@ustb.edu.cn

‡xrchen@scu.edu.cn

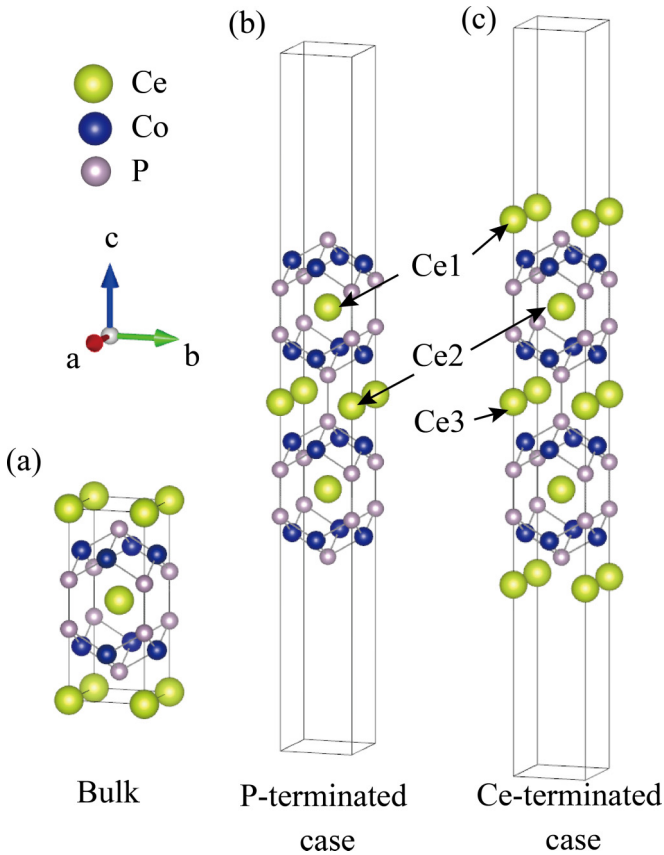


FIG. 1. Crystal structure of CeCo_2P_2 . (a) The bulk, layer structure of (b) the P-terminated slab and (c) the Ce-terminated slab used in the calculation. Green, blue, and pink balls represent Ce, Co, and P atoms, respectively. Ce atoms in the layer structure from outside to inside are labeled as Ce1, Ce2 (and Ce3) in turn.

close to the atomic state. For the P-terminated slab, our results show that the surface Ce-4*f* electrons have a heavy-fermion behavior which is independent of the AFM order of Co at low temperature. We observe the hybridization of surface Ce-4*f*_{5/2} and Co-3*d* conduction bands and a sharper Kondo peak near the Fermi level (E_F) than that in the bulk. In addition, the surface relaxation enhances the Kondo resonance by adjusting the dispersion of the bands near E_F . Second, we find that the flat bands of surface Ce-4*f*_{5/2} of the P-terminated slab are closer to E_F than that of the bulk, while the bands of surface Ce-4*f*_{5/2} of the Ce-terminated slab are much higher than E_F . In addition, we investigate the effect of hybridization on the surface. Finally, after considering the AFM order of Co, we found that the band structure was closer to the ARPES experiment results.

II. THEORETICAL METHOD AND COMPUTATION DETAILS

A. Crystal structures

As shown in Fig. 1(a), in the CeCo_2P_2 crystal, the Ce and Co-P layers are stacked along the *c* axis; thus, we design the P- and Ce-terminated symmetrical slab structure, as shown in Figs. 1(b) and 1(c). A vacuum layer with a height of 20 Å is added to the structure of both slabs. The lattice

parameters of the CeCo_2P_2 bulk used in the calculation come from the experimental data [30]. However, these two symmetrical structures are nonstoichiometric [$(\text{CeCo}_2\text{P}_2)_3\text{Co}_2\text{P}_2$ and $(\text{CeCo}_2\text{P}_2)_4\text{Ce}$ for the P- and Ce-terminated cases, respectively]. This may change the valence state of ions and affect the results. Therefore, we also use a stoichiometric structure, as shown in Fig. S5(a) in the Supplemental Material [33], and perform DFT+DMFT calculations to verify our results of the two symmetrical structures. The detailed results and discussion are displayed in the Supplemental Material [33]. In addition, to compare the electronic band structures of bulk and layers, the conventional Brillouin zone and a similar path are selected in the calculations of the bulk structure, as shown in Fig. 2(a).

For the P- and Ce-terminated slabs, we do not consider the long-range magnetic order in the calculations of DFT and DFT+DMFT. Because of the symmetry of the two structures, the AFM calculations are not convenient. To discuss the influence of magnetism on the electronic structure, we used the asymmetric layer structure, as shown in Fig. 3(a), and perform the DFT calculation of the open core Ce-4*f* with the spin-orbit coupling (SOC) effect.

B. DFT calculations

For DFT calculations, we use the full-potential linearized augmented plane-wave WIEN2K code [34]. The *k* grids were set $12 \times 12 \times 12$ and $20 \times 20 \times 1$ for the bulk and layer structures, respectively, and the radius of the atomic spheres *R* multiplied by the plane-wave cutoff $R_{\text{mt}}K_{\text{max}}$ was set to 8. The exchange-correlation functional is the conventional Perdew-Burke-Ernzerhof (PBE) functional [35], and the SOC effect is considered in a second-order variational manner in the WIEN2K code [34]. We used the DFT+*U* method to relax the ions of the two layer structures by the VASP code with the projector augmented-wave method [36–38], because the relaxation of slabs by DFT+DMFT was too expensive. The cutoff energy is 550 eV. In relaxation, we only consider the on-site interaction parameters of Ce-4*f*, and the Hubbard *U* and Hund exchange *J* were $U = 6.0$ eV and $J = 0.7$ eV, which is a conventional choice [19,39]. Due to the large dispersion of Co-3*d* bands, the Co-3*d* electrons were considered noncorrelated, which is also the same as in the previous work [23]. For the P- and Ce-terminated slabs, we relaxed the ion coordinates of the upper and lower outermost CeCo_2P_2 and $\text{Ce}_2\text{Co}_2\text{P}_2$ molecular layers and fixed the positions of the inner ions and lattice parameters. The results of the Hubbard U_{Ce} and U_{Co} are displayed in the Supplemental Material [33].

C. DFT+DMFT calculations

The DFT+DMFT method combines realistic band-structure calculation by DFT with the nonperturbative many-body treatment of local interaction effects in DMFT. We performed fully charge self-consistent calculations to explore the surface electronic states of the P- and Ce-terminated CeCo_2P_2 structures by the DFT+DMFT method, which has been successfully applied to many strongly correlated electronic materials [39–42]. The implementation of this method

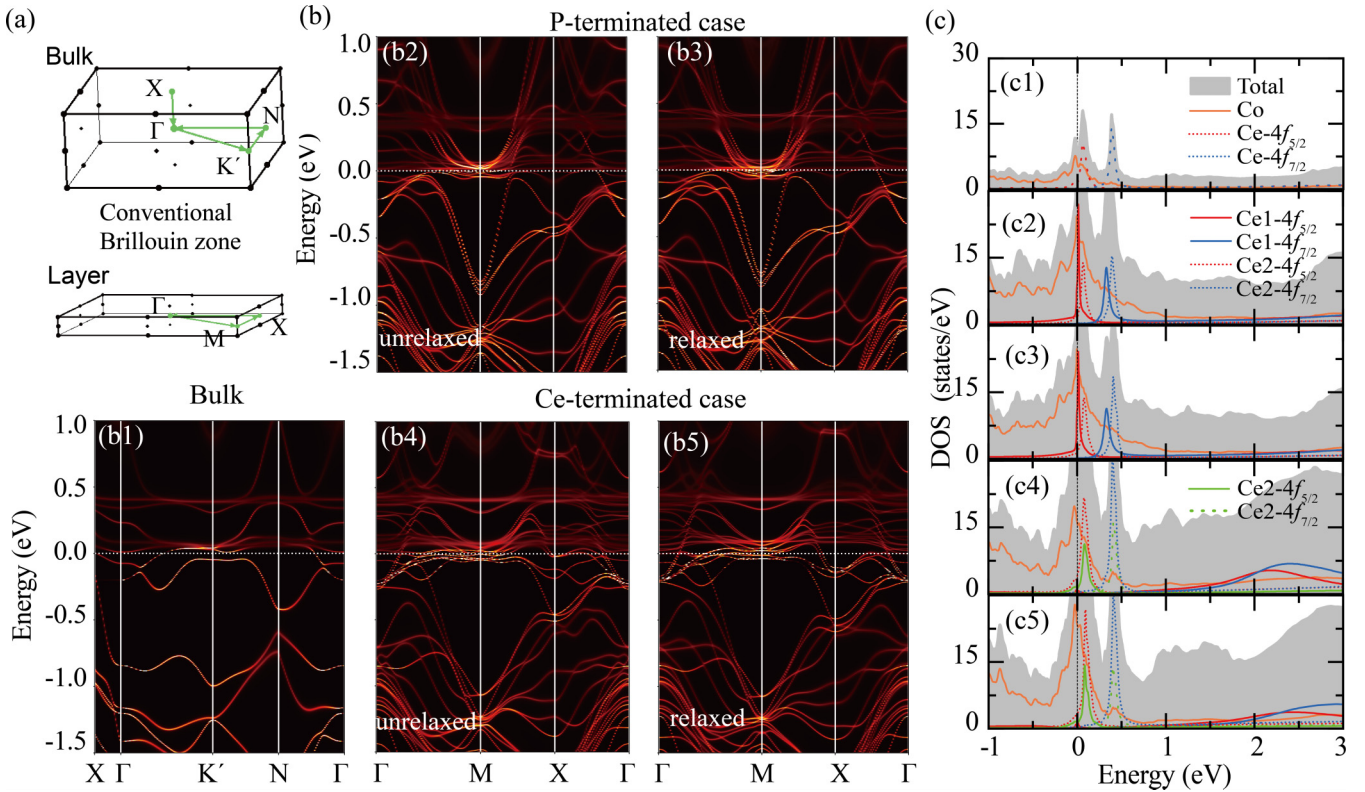


FIG. 2. (a) Brillouin zone of CeCo_2P_2 of bulk and slab structure. For the sake of comparison, the conventional Brillouin zone was selected in calculations of bulk structure. (b) The momentum-resolved spectral functions of (b1) the bulk, (b2) the P-terminated slab, and (b3) the Ce-terminated slab calculated by density functional theory (DFT)+dynamical mean field theory (DMFT) at 20 K. (c) The density of states of (c1) the bulk, (c2) the P-terminated slab, and (c3) the Ce-terminated slab calculated by DFT+DMFT at 20 K.

is divided into DFT and DMFT parts, which are solved separately by using the WIEN2K code and the EDMFTF package [43–46]. The same $R_{\text{mt}}k_{\text{max}}$, k grids, exchange-correlation functional, U , and J are used as in the DFT calculations, and the SOC effect is also considered. We treat the nonequivalent Ce ions in the layer structure as different correlation problems

and deal with them separately. The off-diagonal components of the hybridization function were ignored. It could avoid the negative sign problem and generally does not have a serious impact on the result. We employ the continuous-time quantum Monte Carlo impurity solver to solve the resulting multi-orbital Anderson impurity model [47] and made a truncation

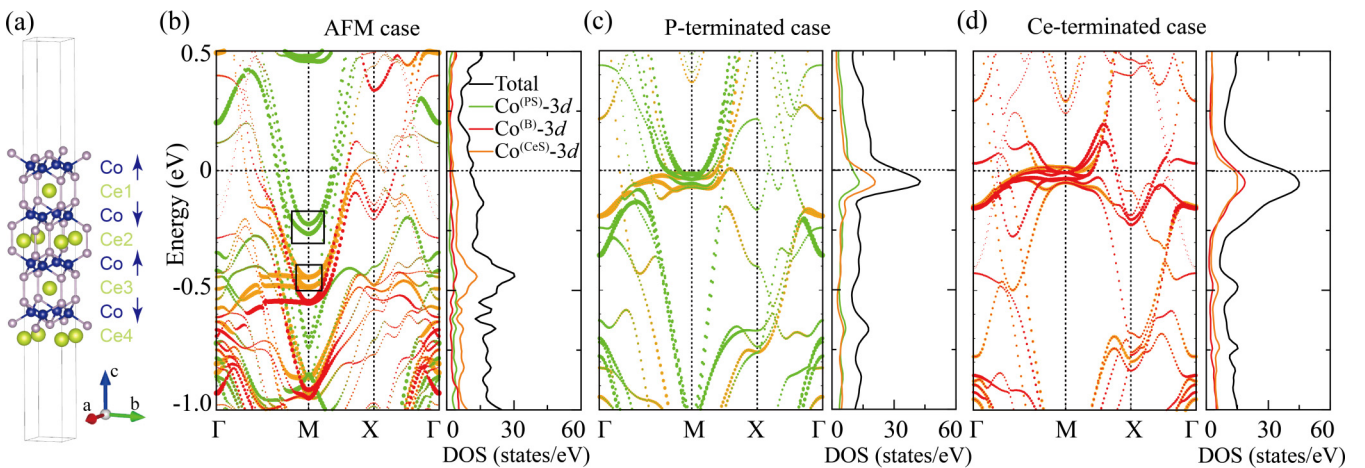


FIG. 3. (a) The antiferromagnetic (AFM) unsymmetrical structure of CeCo_2P_2 . The band structure and density of states (DOS) of (b) AFM, (c) paramagnetic P-terminated, and (d) Ce-terminated cases by density functional theory (DFT) calculations with open-core Ce- $4f$ electrons. The black, green, orange, and red points and lines represent DOS of total, $\text{Co}^{(\text{PS})}-3d$, $\text{Co}^{(\text{CeS})}-3d$, and $\text{Co}^{(\text{B})}-3d$ Ce1- $4f_{5/2}$, respectively [$\text{Co}^{(\text{PS})}$, $\text{Co}^{(\text{CeS})}$, and $\text{Co}^{(\text{B})}$ represent Co of the P-terminated surface, the Ce-terminated surface, and the bulk, respectively].

TABLE I. The distance and change of the outer atoms along the c axis in the P- and Ce-terminated cases after DFT+ U ions relaxation. $d(\alpha-\beta)$ represents the distance between the outer layer α and its adjacent inner layer β . Numbers in parentheses represent the change compared with the distance in the bulk.

Distance (\AA)	Bulk	P-terminated case	Ce-terminated case
$d(\text{Ce-P})$	1.225		0.979 (−20.1%)
$d(\text{P-Co})$	1.158	1.027 (−11.3%)	1.225 (5.7%)
$d(\text{Co-P})$	1.158	1.136 (−1.9%)	1.192 (2.9%)
$d(\text{P-Ce})$	1.225	1.274 (4.0%)	1.165 (−4.9%)
$d(\text{Ce-P})$	1.225	1.173 (−4.3%)	1.217 (−0.7%)

($N \in [0, 1, 2, 3]$) for the local Hilbert space to reduce the computational burden.

III. RESULTS AND DISCUSSION

The stress of ions near the surface of the crystal is different from that of the inside because of the difference of the environment. Thus, we investigated the influence of ionic relaxation near the surface on the structure of the surface. Table I shows the changes of the ionic layer near the surface in the P- and Ce-terminated layer structures relative to the bulk structure. In general, the outermost layers of the two kinds of layer structures moved a large distance to the inner layers, after ionic relaxation (for the P-terminated case, the distance of Co and P in the c -axis direction decreased by 11.3%; for the Ce-terminated case, the distance between the Ce layer and its adjacent P-ion layer decreased by 20%). However, the inner

layer structure moves less than the outermost layer. In the study of a Ce-base material with the same structure, CeRh_2Si_2 [19], a similar influence of the ionic relaxation on the structure was also observed. Obviously, the ionic relaxation will change the electronic structure of surface states, as we will discuss later.

To study the electronic structure of the bulk and two kinds of layer structures, we perform the DFT+DMFT calculations for them at different temperatures. Figures 2(b) and 2(c) show the momentum-resolved spectral functions and density of states (DOS) of the bulk and layer structures at 20 K. For the CeCo_2P_2 bulk, the conduction band mainly consists of Co-3d electrons, and Ce-4f flat bands are formed at ~ 0.1 and ~ 0.4 eV above E_F , as shown in Figs. 2(b1) and 2(c1). In addition, the clear hybridization between Ce-4f and the conduction electrons can be observed. For the two kinds of layer structures, similar bands of the bulk materials could be observed in the spectral functions, as shown in Fig. 2(b). The flat bands of internal Ce-4f $_{5/2}$ and Ce-4f $_{7/2}$ can also be observed at ~ 0.1 and ~ 0.4 eV, which are consistent with that of the bulk. These results show that the properties of internal Ce in the layer structure we used are basically the same as those in the bulk. As shown in Figs. 2(b2) and 2(c2), for the P-terminated case, the 4f flat bands of Ce1 are closer to E_F than that of the bulk, and the flat bands of Ce1-4f $_{5/2}$ and Ce1-4f $_{7/2}$ are located ~ 0.015 and ~ 0.3 eV, respectively. Otherwise, the DOS peak of Ce1-4f $_{5/2}$ is much sharper than that of Ce2-4f $_{5/2}$. However, for the Ce-terminated case, the 4f bands of Ce1 are much higher than E_F [the peaks of Ce1-4f $_{5/2}$ and Ce1-4f $_{7/2}$ in DOS are located at ~ 2.2 and ~ 2.4 eV, respectively, as shown in Fig. 2(c3)], and the width of the peak in DOS is very large. The strength of hybridization

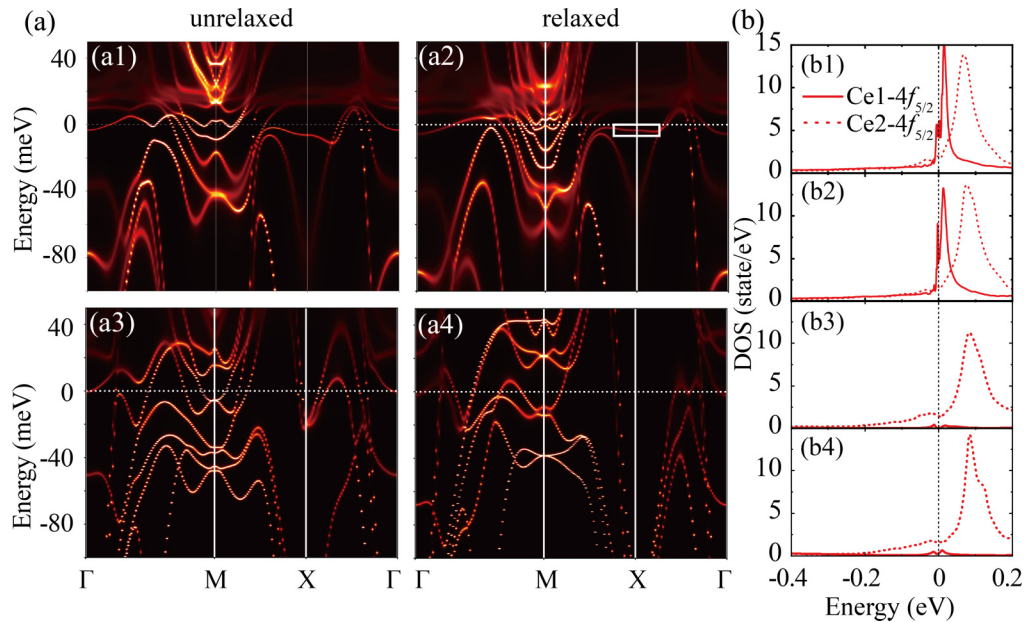


FIG. 4. (a) The momentum-resolved spectral functions and (b) density of states (DOS) near E_F calculated by density functional theory (DFT)+dynamical mean field theory (DMFT) at 20 K. Panels (a1), (b1) and (a3), (b3) are the results of unrelaxed crystal structures of the P- and Ce-terminated cases, respectively. Panels (a2), (b2) and (a4), (b4) are the results of unrelaxed crystal structures of the P- and Ce-terminated cases, respectively. The red solid line and dotted line represent the DOS of Ce1-4f $_{5/2}$ (outer Ce) and Ce2-4f $_{5/2}$ (inner Ce), respectively. A clear flat band can be observed in the white rectangle in (a2).

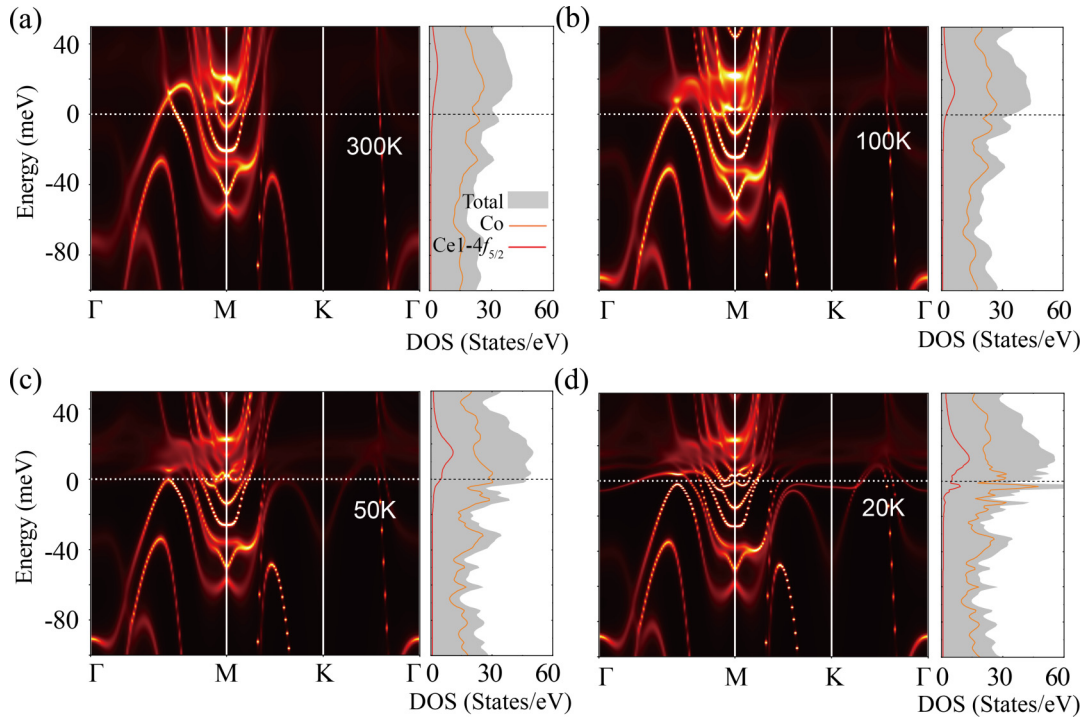


FIG. 5. The momentum-resolved spectral functions and density of states (DOS) near E_F of the P-terminated slab after relaxed calculated by density functional theory (DFT)+dynamical mean field theory (DMFT) at (a) 300 K, (b) 100 K, (c) 50 K, and (d) 20 K. The gray area and orange and red solid lines represent DOS of total, Co-3d, and Ce1-4 $f_{5/2}$, respectively.

is closely related to the Kondo peak at E_F , and the sharper Kondo peak generally corresponds to the stronger hybridization. This indicates that the correlation effect of Ce1 in the P-terminated slab is much stronger than that in the Ce-terminated case. In addition, our results indicate that the magnetic order of Co ions near the surface was not responsible for the strong correlation effect of Ce-4 f near the surface.

In fact, our CeCo₂P₂ slab structure exposing a face bearing a net charge is unstable due to the dipole moment perpendicular to the surface, the so-called polar catastrophe. The Ce-terminated slab surface is more unstable than the P-terminated slab because the surface Ce ions are in direct contact with vacuum. We also find in self-consistent computation that the Ce interface structure requires more iterations to converge. The samples of Poelchen *et al.* [23] proved to be P terminated, suggesting that the P-terminated structure is more stable. The effects of structural reconstructions deserve further considerations.

To study the effect of relaxation on the electronic structure more clearly, we calculate the spectral function and DOS near E_F of the two kinds of layer structures before and after the relaxation at 20 K (see in Fig. 4). As shown in Figs. 4(a1) and 4(a2), for the P-terminated case, there are clear Ce1-4 $f_{5/2}$ flat bands at ~ 15 meV which are closer to E_F than Ce2-4 $f_{5/2}$ and a clear hybridization between Ce1-4 $f_{5/2}$ and conduction electrons. In addition, the bands near E_F were renormalized after relaxation; for example, the band at the X point [white rectangle in Fig. 4(a2)] becomes flatter. This corresponds to the sharp Ce1-4 $f_{5/2}$ peak of DOS at E_F in Fig. 4(b2). In addition, the relaxation causes a large movement of the band at ~ -60 meV in the Γ -M path. The results of DOS in Fig. 4(a2)

showed that the main component of these bands is Co-3d. The relaxation reduces the bond length of Co-P near the surface, which may be the reason for the band renormalization. In addition, the heights of the Kondo peaks of Ce1-4 $f_{5/2}$ and Ce2-4 $f_{5/2}$ are basically the same, but the width of the Kondo peak of Ce1-4 $f_{5/2}$ is obviously lower than that of Ce2. However, for the Ce-terminated case, the energy of the Ce1-4 f flat bands is far away from E_F , as shown in Figs. 4(a1) and 4(a2) [23]. After relaxations, the bands are also renormalized after relaxation; the bands at the X and M points near E_F moved. There is a very small peak of Ce1-4 $f_{5/2}$ on both sides of E_F . For the Ce-terminated slab, Ce1 ions directly contact with vacuum, and that causes its Kondo peak to be very different from that of Ce2. Compared with the bulk, the Sommerfeld coefficient γ (~ 23.7 mJ mol⁻¹ K⁻²) estimated by DOS of the P-terminated slab is significantly improved, and relaxation improves γ (~ 27.0 mJ mol⁻¹ K⁻²) significantly. If the temperature is lower, the Sommerfeld coefficient may become larger.

The results of ARPES by Poelchen *et al.* [23] captured four bands with surface features: the α and β bands were located at ~ -0.05 and ~ -0.25 eV at the M point with parabolic shapes, the δ band was located near E_F at the Γ point, and the γ band was located at ~ -0.05 eV between the Γ and M points. For the P-terminated case, our results of DFT (see Fig. S1 in the Supplemental Material [33]) and DFT+DMFT successfully capture the characteristics of the δ and γ bands, but only some bands are observed at ~ -0.05 eV at the M point. This may be because of the AFM order of Co ions. Thus, we built the asymmetric layer structure with AFM order of Co ions, as shown in Fig. 3(a). Since the magnetic calculations

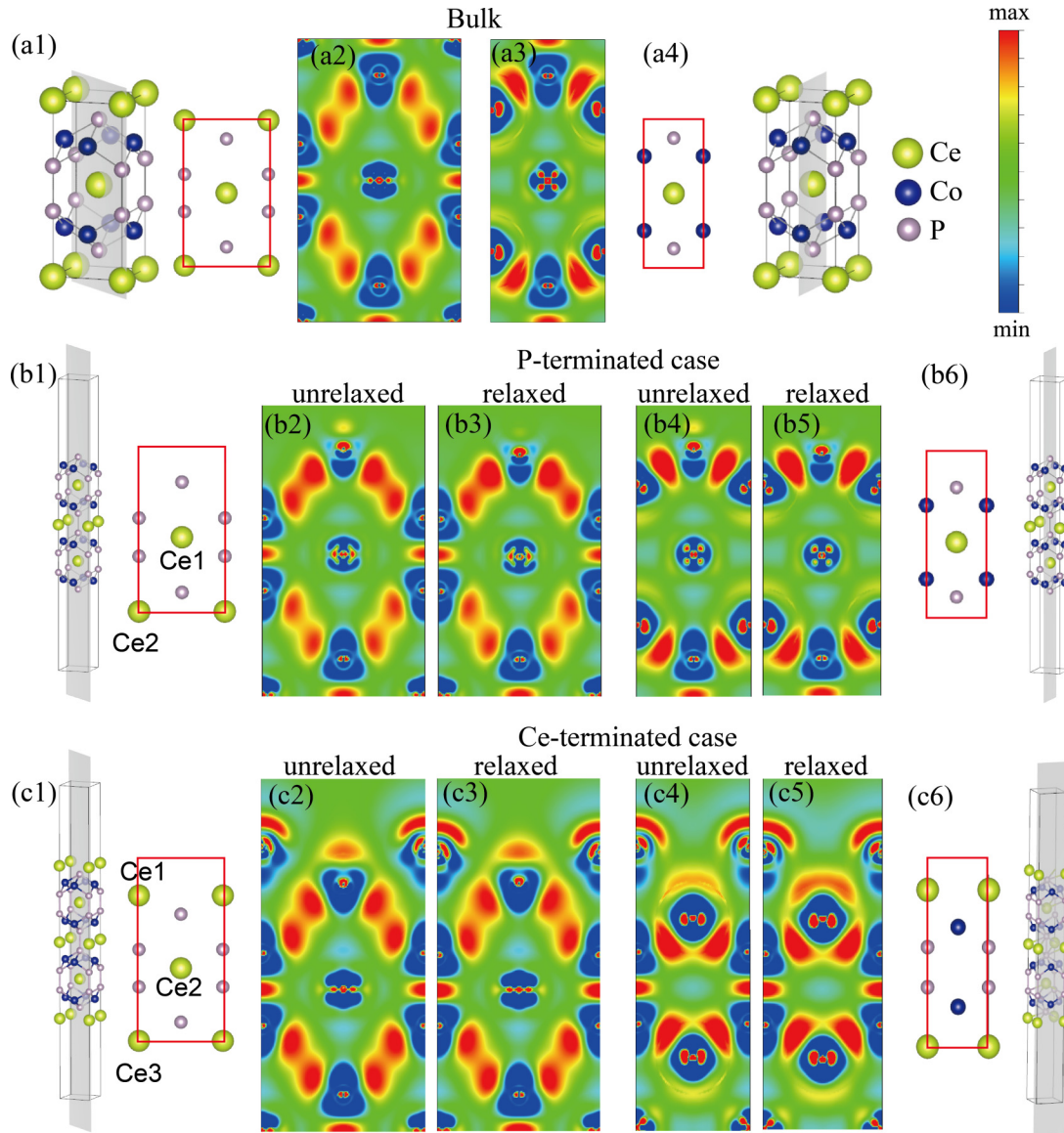


FIG. 6. The difference of electron density between results of density functional theory (DFT)+dynamical mean field theory (DMFT) calculation at 20 K and the superposition of spherical atomic electron density. Panels (a2), (a3); (b2)–(b5); and (c2)–(c5) are the results of the bulk, P-, and Ce-terminated cases, respectively. Panels (a1), (a4); (b1), (b6); and (c1), (c6) show the definition of the slices used in (a2), (a3); (b2)–(b5); and (c2)–(c5), respectively. The warm and cold colors indicate that the electron density increases and decreases, respectively.

of DFT+DMFT were too expensive, we performed the AFM DFT calculations with open-core Ce-4*f* states. Figures 3(b)–3(d) show the band structure and DOS of the AFM and the P- and Ce-terminated slabs. For the P-terminated slab, compared with Fig. S1 in the Supplemental Material [33] and Fig. 2, the Co-3*d* bands of DFT with open-core were basically consistent with that of normal DFT and DFT+DMFT. At the *M* point, there were Co-3*d* bands at ~ -0.05 eV. For the AFM slab, as shown in black rectangles of Fig. 3(b), the bands at the *M* point move to ~ -0.2 and ~ -0.45 eV, with obvious parabolic shape. In addition, the bands in rectangles are mainly contributed by Co-3*d* near the P-terminated surface and internal Co-3*d*, which is consistent with our conclusions. These characteristics were the same as those of ARPES experiments, and the differences of energy may be caused by the ionic bond length [23]. Therefore, for the results to be

in better agreement with the experiment, it is necessary to consider both the magnetism of Co and the strong correlation effect of Ce-4*f*. Our results indicated that the heavy-fermion behavior of P-terminated Ce-4*f* and the AFM order of Co ions are independent.

After determining that the surface of the P-terminated case has a stronger correlation effect, we calculated the spectral function and DOS of the P-terminated case near E_F at different temperatures (see in Fig. 5). At 300 K, the conduction band passing through E_F can be observed, which is mainly composed of Co-3*d*. As the temperature decreases to 50 K, the Ce1-4*f*_{5/2} flat bands and its hybridization with conduction bands appear at ~ 15 meV, as shown in Figs. 5(a)–5(c). When the temperature drops to 20 K, the hybridization is further enhanced, and the Kondo peak appears near E_F , as shown in Fig. 5(d).

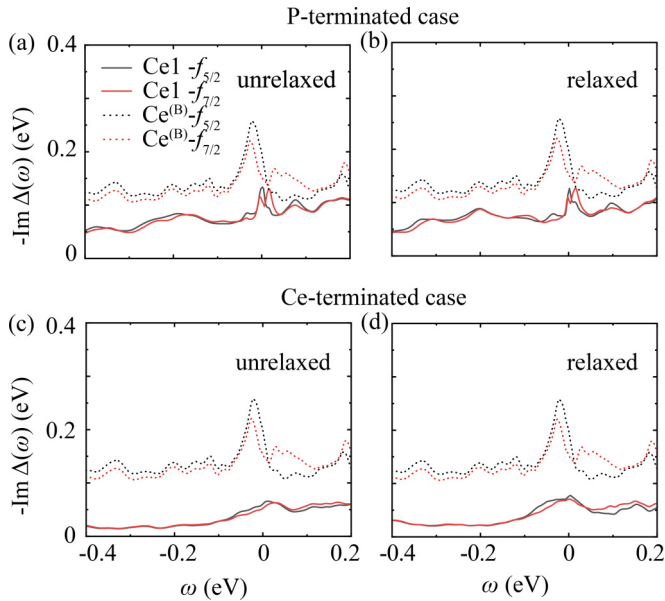


FIG. 7. The imaginary part of hybridization function on real frequency $\text{Im}\Delta(\omega)$ of the P- and Ce-terminated slabs at 20 K, respectively. The red and black dotted lines represent $\text{Ce-}4f_{5/2}$ and $\text{Ce-}4f_{7/2}$ in the bulk structure. The red and black lines represent $4f_{5/2}$ and $4f_{7/2}$ electrons of Ce1 in the four slabs. (a) and (c) Results of unrelaxed crystal structures of the P- and Ce-terminated slabs, respectively. (b) and (d) Results of unrelaxed crystal structures of the P- and Ce-terminated cases, respectively.

To better understand the electronic structure of Ce in the two structures, we calculate the difference of the electron density between results of DFT+DMFT calculation at 20 K and the superposition of the spherical atomic electron density (see in Fig. 6). The electrons on the Ce atom transfer to the environment composed of the Co-P layer. As shown in Figs. 6(a2), 6(b2), 6(b3), 6(c2), and 6(c3), the charge density around Ce2 ions in two kinds of layer structures and Ce in the bulk are basically the same, while the charge density around Ce1, especially the Ce-terminated case, are different from that of the bulk. For the P-terminated case, as shown in Figs. 6(b4) and 6(b5), the charge density around the Co ions near the surface is greatly different from that of the inner layer, so its hybridization with Ce1 should also be different from that of Ce in the bulk. However, for the Ce-terminated case, the charge around Ce1 is obviously more itinerant than Ce2 [see in the Figs. 6(c4) and 6(c5)]. In addition, a hemispherical electron density gathered on the surface contacts the vacuum layer, which means that it may be closer to the atomic state and its hybridization is much weaker than that of the bulk. On the other hand, the electron density around the ions does not seem to change significantly after ion relaxation in the P- and Ce-terminated cases.

Furthermore, we calculated the hybridization functions of $\text{Ce-}4f$ with two kinds of layer structures using the maximum entropy method [48]. The results were shown

in Fig. 7. The imaginary part of the hybridization function can be used to describe the strength of hybridization: $\text{Im}\Delta(\omega) = -\pi \sum_k |V_k|^2 \delta(\omega - \epsilon_k)$. As shown in Figs. 7(a) and 7(b), for the P-terminated slab, although the imaginary part of the hybridization function $\text{Im}\Delta(\omega)$ of $\text{Ce1-}4f_{5/2}$ is lower than that of the bulk, there was a sharp peak of $\text{Ce1-}4f_{5/2}$ at $\omega = 0$, and the flat bands of $\text{Ce1-}4f_{5/2}$ are closer to E_F than Ce in the bulk. However, for the Ce-terminated slab, the $\text{Im}\Delta(\omega)$ of $\text{Ce1-}4f_{5/2}$ is much lower than that of the bulk because the Ce1 ions are closer to the atomic state.

IV. CONCLUSIONS

In summary, we investigated the electronic structures of the surface states of CeCo_2P_2 using DFT and DFT+DMFT methods, by compared with the results of the bulk. First, the spectrum function of the P-terminated slab at low temperature by DFT+DMFT indicate that $\text{Ce1-}4f$ near the surface has heavy-fermion behavior, and it was independent of the AFM order of Co ions. As the temperature decreases, the flat bands of $\text{Ce-}4f_{5/2}$ near the surface of the P-terminated case begin to hybridize with the Co-3d conduction bands at 50 K, and a sharp Kondo peak can be observed at 20 K. In addition, the relaxation of surface ions changed the bond length and further renormalized the bands and enhanced the correlation effect. Second, for the P-terminated layer structure, the $4f_{5/2}$ flat bands of Ce near the surface at low temperature are closer to E_F than that of the bulk (~ 0.015 and ~ 0.1 eV above E_F for the P-terminated slab and the bulk, respectively). However, for the Ce-terminated slab, the energy level of $\text{Ce1-}4f_{5/2}$ on the surface is far away from E_F (~ 2.2 eV above E_F) because the Ce ions on the surface are in contact with the vacuum and closer to the atomic state. Also, the strength of hybridization of the surface $\text{Ce1-}4f$ with Co-3d conduction band in the P-terminated slab is much stronger than that in the Ce-terminated case, which is the reason for the difference of their surface states. Finally, we found that the difference between our DFT+DMFT results and the ARPES experiment may be due to the AFM order of Co ions, but the heavy-fermion behavior of the surface state is not caused by AFM order. These results show that CeCo_2P_2 is an ideal material for studying interlayer coupling between two-dimensional Kondo lattices and magnetic layers. Our results also verify the reliability of the DFT+DMFT method in studying the surface electronic states of strongly correlated materials.

ACKNOWLEDGMENTS

This paper was supported by the National Natural Science Foundation of China (Grants No. 12074274 and No. 12204033), the Young Elite Scientist Sponsorship Program by BAST (Grant No. BYESS2023301), and the Natural Science Foundation of Chongqing City (Grant No. cstc2020jcyj-msxmX0616).

There are no conflicts of interest to declare.

[1] G. Chen, S. Ohara, M. Hedo, Y. Uwatoko, K. Saito, M. Sorai, and I. Sakamoto, *J. Phys. Soc. Jpn.* **71**, 2836 (2002).

[2] P. Gegenwart, Q. Si, and F. Steglich, *Nat. Phys.* **4**, 186 (2008).

- [3] Y. Kohori, Y. Yamato, Y. Iwamoto, T. Kohara, E. D. Bauer, M. B. Maple, and J. L. Sarrao, *Phys. Rev. B* **64**, 134526 (2001).
- [4] R. Movshovich, T. Graf, D. Mandrus, J. D. Thompson, J. L. Smith, and Z. Fisk, *Phys. Rev. B* **53**, 8241 (1996).
- [5] M. Sigrist and K. Ueda, *Rev. Mod. Phys.* **63**, 239 (1991).
- [6] G. R. Stewart, *Rev. Mod. Phys.* **56**, 755 (1984).
- [7] G. R. Stewart, Z. Fisk, and M. S. Wire, *Phys. Rev. B* **30**, 482 (1984).
- [8] S. L. Bud'ko, M. B. Fontes, M. A. Continentino, and E. Baggio-Saitovitch, *Phys. B: Condens. Matter* **217**, 111 (1996).
- [9] F. Lu, J.-Z. Zhao, H. Weng, Z. Fang, and X. Dai, *Phys. Rev. Lett.* **110**, 096401 (2013).
- [10] M. Pothoff and W. Nolting, *Phys. Rev. B* **59**, 2549 (1999).
- [11] M. Pothoff and W. Nolting, *Phys. Rev. B* **60**, 7834 (1999).
- [12] S. Keshavarz, Y. O. Kvashnin, I. Di Marco, A. Delin, M. I. Katsnelson, A. I. Lichtenstein, and O. Eriksson, *Phys. Rev. B* **92**, 165129 (2015).
- [13] G. Lantz, M. Hajlaoui, E. Papalazarou, V. L. R. Jacques, A. Mazzotti, M. Marsi, S. Lupi, M. Amati, L. Gregoratti, L. Si *et al.*, *Phys. Rev. Lett.* **115**, 236802 (2015).
- [14] F. Lechermann, H. O. Jeschke, A. J. Kim, S. Backes, and R. Valentí, *Phys. Rev. B* **93**, 121103(R) (2016).
- [15] I. Leonov and S. Biermann, *Phys. Rev. B* **103**, 165108 (2021).
- [16] D.-C. Ryu, C.-J. Kang, J. Kim, K. Kim, G. Kotliar, J. S. Kang, J. D. Denlinger, and B. I. Min, *Phys. Rev. B* **103**, 125101 (2021).
- [17] X. Ma, G. Wang, R. Liu, T. Yu, Y. Peng, P. Zheng, and Z. Yin, *Phys. Rev. B* **106**, 115114 (2022).
- [18] S. Patil, A. Generalov, M. Güttler, P. Kushwaha, A. Chikina, K. Kummer, T. C. Rödel, A. F. Santander-Syro, N. Caroca-Canales, C. Geibel *et al.*, *Nat. Commun.* **7**, 11029 (2016).
- [19] Y.-C. Wang, Y.-J. Xu, Y. Liu, X.-J. Han, X.-G. Zhu, Y.-f. Yang, Y. Bi, H.-F. Liu, and H.-F. Song, *Phys. Rev. B* **103**, 165140 (2021).
- [20] C. E. Matt, H. Pirie, A. Soumyanarayanan, Y. He, M. M. Yee, P. Chen, Y. Liu, D. T. Larson, W. S. Paz, J. J. Palacios *et al.*, *Phys. Rev. B* **101**, 085142 (2020).
- [21] H. Pirie, Y. Liu, A. Soumyanarayanan, P. Chen, Y. He, M. M. Yee, P. F. S. Rosa, J. D. Thompson, D.-J. Kim, Z. Fisk *et al.*, *Nat. Phys.* **16**, 52 (2020).
- [22] A. V. Tarasov, M. Mende, K. Ali, G. Poelchen, S. Schulz, O. Y. Vilkov, K. A. Bokai, M. Muntwiler, V. Mandic, C. Laubschat *et al.*, *Surf. Interfaces* **32**, 102126 (2022).
- [23] G. Poelchen, I. P. Rusinov, S. Schulz, M. Güttler, M. Mende, A. Generalov, D. Y. Usachov, S. Danzenbächer, J. Hellwig, M. Peters *et al.*, *ACS Nano* **16**, 3573 (2022).
- [24] M. Güttler, A. Generalov, M. M. Otrokov, K. Kummer, K. Kliemt, A. Fedorov, A. Chikina, S. Danzenbächer, S. Schulz, E. V. Chulkov *et al.*, *Sci. Rep.* **6**, 24254 (2016).
- [25] A. Generalov, J. Falke, I. A. Nechaev, M. M. Otrokov, M. Güttler, A. Chikina, K. Kliemt, S. Seiro, K. Kummer, S. Danzenbächer *et al.*, *Phys. Rev. B* **98**, 115157 (2018).
- [26] S. Schulz, I. A. Nechaev, M. Güttler, G. Poelchen, A. Generalov, S. Danzenbächer, A. Chikina, S. Seiro, K. Kliemt, A. Y. Vyazovskaya *et al.*, *npj Quantum Mater.* **4**, 26 (2019).
- [27] G. Poelchen, S. Schulz, M. Mende, M. Güttler, A. Generalov, A. V. Fedorov, N. Caroca-Canales, C. Geibel, K. Kliemt, C. Krellner *et al.*, *npj Quantum Mater.* **5**, 70 (2020).
- [28] D. Y. Usachov, I. A. Nechaev, G. Poelchen, M. Güttler, E. E. Krasovskii, S. Schulz, A. Generalov, K. Kliemt, A. Kraiker, C. Krellner *et al.*, *Phys. Rev. Lett.* **124**, 237202 (2020).
- [29] D. Y. Usachov, A. V. Tarasov, S. Schulz, K. A. Bokai, I. I. Tupitsyn, G. Poelchen, S. Seiro, N. Caroca-Canales, K. Kliemt, M. Mende *et al.*, *Phys. Rev. B* **102**, 205102 (2020).
- [30] M. Reehuis, W. Jeitschko, G. Kotzyba, B. Zimmer, and X. Hu, *J. Alloys Compd.* **266**, 54 (1998).
- [31] A. Teruya, A. Nakamura, T. Takeuchi, F. Honda, D. Aoki, H. Harima, K. Uchima, M. Hedo, T. Nakama, and Y. Ōnuki, *Phys. Procedia* **75**, 876 (2015).
- [32] Y. Xu, L. Elcoro, Z.-D. Song, B. J. Wieder, M. G. Vergniory, N. Regnault, Y. Chen, C. Felser, and B. A. Bernevig, *Nature (London)* **586**, 702 (2020).
- [33] See Supplemental Material at <https://link.aps.org/supplemental/10.1103/PhysRevB.107.195440> for additional calculations and analyses.
- [34] P. Blaha, K. Schwarz, F. Tran, R. Laskowski, G. K. H. Madsen, and L. D. Marks, *J. Chem. Phys.* **152**, 074101 (2020).
- [35] J. P. Perdew, K. Burke, and M. Ernzerhof, *Phys. Rev. Lett.* **77**, 3865 (1996).
- [36] V. I. Anisimov, J. Zaanen, and O. K. Andersen, *Phys. Rev. B* **44**, 943 (1991).
- [37] V. I. Anisimov, I. V. Solovyev, M. A. Korotin, M. T. Czyzyk, and G. A. Sawatzky, *Phys. Rev. B* **48**, 16929 (1993).
- [38] J. Hafner, *J. Comput. Chem.* **29**, 2044 (2008).
- [39] H. Lu and L. Huang, *Phys. Rev. B* **98**, 195102 (2018).
- [40] S. Mandal, K. Haule, K. M. Rabe, and D. Vanderbilt, *npj Comput. Mater.* **5**, 115 (2019).
- [41] Y. Xu, Y. Sheng, and Y.-F. Yang, *Phys. Rev. Lett.* **123**, 217002 (2019).
- [42] C. Cao, G.-X. Zhi, and J.-X. Zhu, *Phys. Rev. Lett.* **124**, 166403 (2020).
- [43] G. Kotliar, S. Y. Savrasov, K. Haule, V. S. Oudovenko, O. Parcollet, and C. A. Marianetti, *Rev. Mod. Phys.* **78**, 865 (2006).
- [44] J. H. Shim, K. Haule, and G. Kotliar, *Science* **318**, 1615 (2007).
- [45] K. Haule, J. H. Shim, and G. Kotliar, *Phys. Rev. Lett.* **100**, 226402 (2008).
- [46] K. Haule, *Phys. Rev. Lett.* **115**, 196403 (2015).
- [47] K. Haule, *Phys. Rev. B* **75**, 155113 (2007).
- [48] M. Jarrell and J. E. Gubernatis, *Phys. Rep.* **269**, 133 (1996).